Journal of Geoscience and Environment Protection, 2023, 11, 216-232
https://www.scirp.org/journal/gep
ISSN Online: 2327-4344
ISSN Print: 2327-4336

ASTER Data Processing by Discrete Wavelets Transform and Band Ratio Techniques for the Identification of Lineaments and Hydrothermal Alteration Zones in Poli, North Cameroon

Mohamadou Ahamadou[1*], May Nome Stella[1,2], Meying Arsène[1]

[1]School of Geology and Mining Engineering, University of Ngaoundéré, Ngaoundéré, Cameroon
[2]Centre for Geological and Mining Research, Garoua, Cameroon
Email: *ahamadoumohamadou@yahoo.com

How to cite this paper: Ahamadou, M., Stella, M. N., & Arsène, M. (2023). ASTER Data Processing by Discrete Wavelets Transform and Band Ratio Techniques for the Identification of Lineaments and Hydrothermal Alteration Zones in Poli, North Cameroon. *Journal of Geoscience and Environment Protection, 11,* 216-232.
https://doi.org/10.4236/gep.2023.119014

Received: August 5, 2023
Accepted: September 22, 2023
Published: September 25, 2023

Abstract

The aim of this study is to carry out hydrothermal alteration mapping and structural mapping using ASTER images in order to identify indices that could guide mining exploration work in the Poli area and its surroundings. To achieve this, the ASTER images were first preprocessed to correct atmospheric effects and remove vegetation influence. Secondly, a lineament mapping was conducted by applying Discrete Wavelet Transform (DWT) algorithms to the First Principal Component Analysis (PCA1) of Visible Near-Infrared (VNIR) and Shortwave Infrared (SWIR) bands. Lastly, band ratio methods were applied to the VNIR, SWIR, and Thermal Infrared (TIR) bands to determine indices of iron oxides/hydroxides (hematite and limonite), hydroxyl-bearing minerals (chlorite, epidote, and muscovite), and the quartz index. The results obtained showed that the lineaments were mainly oriented NE-SW, ENE-WSW, and E-W, with NE-SW being the most predominant direction. Concerning hydrothermal alteration, the identified indices covered almost the entire study area and showed a strong correlation with lithological data. Overlaying the obtained lineaments with the hydrothermal alteration indices revealed a significant correlation between existing mining indices and those observed in the field. Mineralized zones generally coincided with areas of high lineament density exhibiting significant hydrothermal alteration. Based on the correlation between existing mining indices and the results of hydrothermal and structural mapping, the results obtained can then be used as a reference document for any mining exploration in the study area.

Keywords

Discrete Wavelets Transform, Band Ratio, Lineaments, Hydrothermal Alteration

1. Introduction

For several decades, the advancement of precise remote sensing technology has significantly impacted the progress of numerous nations. This influence has been most notable in enhancing understanding and insights across crucial economic sectors, including mining, oil exploration, agriculture, water resource management, environmental monitoring, urban development, and disaster preparedness, among others. The utilization of remotely acquired data offers a unique advantage by providing a comprehensive overview of extensive regions, unencumbered by limitations that on-site investigations often face, such as constrained study areas, logistical challenges, unpredictable climatic conditions, natural disasters, and socio-political instability. As a result, surveys conducted through remote sensing methods demand less time and financial resources while delivering superior outcomes compared to traditional ground-based research, when effectively employed. In the context of Cameroon, a significant portion of the country remains unexplored due to various factors, including the prohibitive costs associated with direct mineral exploration. This holds true for the North Cameroon region, particularly in the Poli area, where exploration efforts have remained limited despite the region's abundant mineral potential. To capitalize on the advantages offered by remote sensing imagery, we have leveraged the growing popularity of ASTER images (Deroin, 2019; Ouhoussa et al., 2022) for conducting reconnaissance mapping in the Poli area. The Poli area is located in the Northern Cameroon region, bounded by the latitude coordinates 08˚10'39" and 08˚34'22" North, as well as longitudes 13˚03' and 13˚31' East. This area covers an area of 2298.3 km^2, with a length of 52.212 km and a width of 43.717 km. Previous works in this area associate the study area with the Poli group (Bouyo et al., 2015; Negue et al., 2017). The Poli group is characterized by the presence of metavolcanic and metasedimentary formations. These authors also mentioned the presence of gold and uranium mineralizations associated with geological structures such as faults and fractures in the region. The most recent remote sensing works in this study area, notably Anaba Fotze et al. (2019) and Ketchaya et al. (2021) focused on mapping regional hydrothermal and structural alteration using Landsat OLI 8 images. However, to provide more accurate and localized information on hydrothermal alteration and structural mapping, ASTER data, which offers better precision and efficiency compared to Landsat OLI 8 (Baid et al., 2023), was used. This approach is innovative in this context as it has never been used before in this study area. Thus, to achieve the set objective, the present work is divided into two main goals. First, mapping of lineaments will be performed using the wavelet transform of ASTER images. Second, mapping of hydrothermal alteration indices will be conducted using band ratios and spectral analysis to identify areas rich in iron oxides/hydroxides and hydroxyl-bearing minerals.

2. Geological and Mining Setting

The geological configuration of Cameroon reveals its location to the north of the

stable Congo craton. According to Penaye et al. (1993), Toteu et al. (2001) and Njanko et al. (2010), Cameroon is part of the Central Africa Fold Belt, a mega-chain that stretches over 5000 km in length and 3000 km in width (Bouyo et al., 2013). This belt mainly comprises large blocks of Precambrian rocks separated by extensive areas of metamorphosed sediments (Lasserre & Doba, 1979; Bessoles & Trompette, 1980; Affaton et al., 1991). The Central Africa Fold Belt in Cameroon is divided into three main domains based on geochemical, geophysical, and geological characteristics: the Southern Cameroon Domain (SCD), the Northern Cameroon Domain (NCD), and the Central Domain, also known as the Adamaoua-Yade Domain (AYD) (**Figure 1(a)**) (Ngnotué et al., 2000; Toteu et al., 2004; Nzenti et al., 2006). The Poli zone belongs to the Northern Cameroon Domain of the Central Africa Fold Belt in Cameroon (Penaye et al., 1993; Toteu et al., 2001; Njanko et al., 2010). According to Abdelsalam et al. (2002, 2011), the NCD resulted from the collision between the AYD and the Sahara metacraton. The NCD and AYD are separated by the sinistral Tcholliré Shear Zone (TSZ) trending NE-SW. The study area is located west of the TSZ and belongs to the Poli group. According to Penaye et al. (2006) and Pinna et al. (1994), this group corresponds to an early back-arc orogenic basin formed around 700 to 665 Ma. It is predominantly composed of metavolcanic

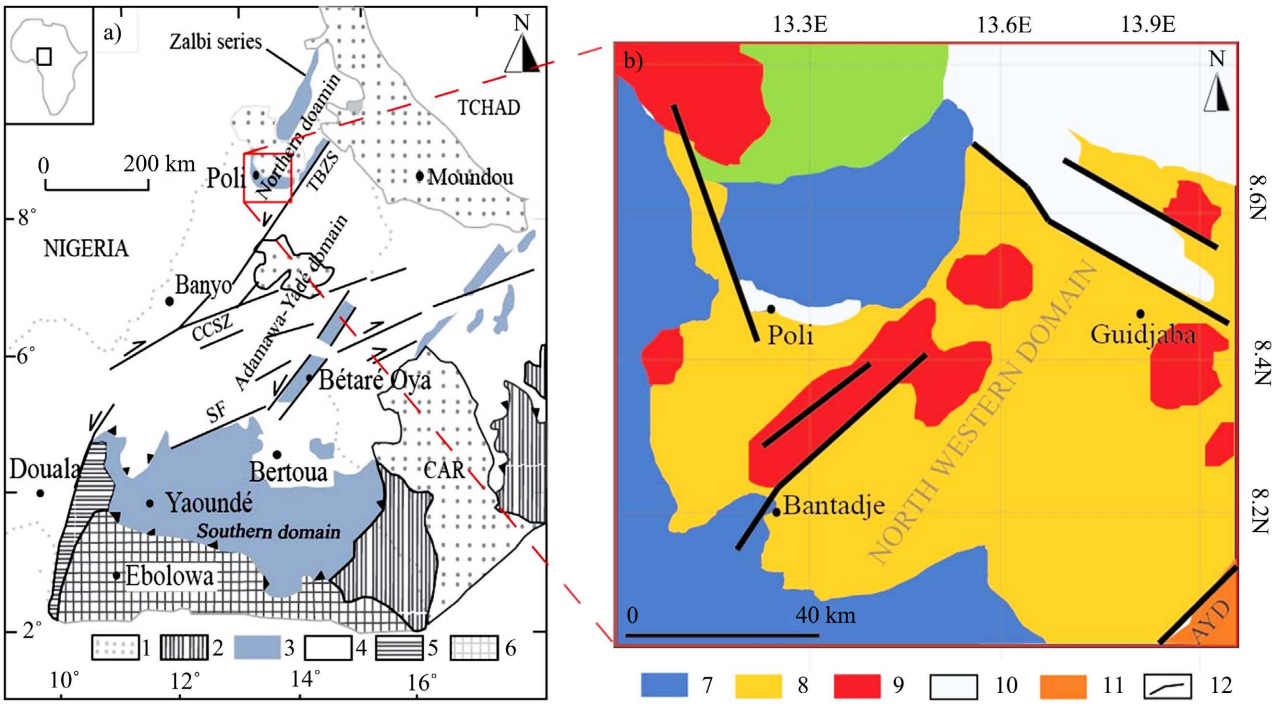

Figure 1. Geological sketch map of the Central African Fold Belt (CAFB) showing location of Neoproterozoic supra crustal sequences: (1) Post-Pan-African cover; (2) Platform cover on the Congo craton; (3) Neoproterozoic units; (4) Granitoids, gneisses and migmatites of various ages of the basement complex; (5) Palaeoproterozoic Nyong Group; (6) Congo craton. The dotted line represents political boundaries. TBSZ: Tchollire-Banyo Shear Zone; CCSZ: Central Cameroonian Shear Zone; SF: Sanaga Fault. The Adamawa-Yadé Domain (AYD) extends between the TBSZ and the Yaoundé Group: (7) Gneiss; (8) Volcano-sedimentary rocks; (9) Late to post-Pan-African tectonics granitoids; (10) Post-Pan-African sediments, (11) AYD; (12) Faults. Source: Penaye et al. (2006).

and metasedimentary formations (**Figure 1(b)**) (Penaye et al., 2006). The metavolcanic formations consist mainly of sodic rhyolites and tholeiitic basalts, while the metasedimentary formations are predominantly composed of volcanogenic clastic rocks like tuffs or variably reworked clastic rocks of intermediate composition such as meta grey wackes (Toteu et al., 2006). From a mining perspective, the Poli zone is characterized mainly by the presence of uranium mineralizations around the towns of Poli, Bantadjé, and Salaki. According to Kouske et al. (2012), uranium mineralization is a result of Na-Ca metasomatism and is associated with brittle faults that cross-cut ENE trending ductile shear zones. Gold is also found in the localities of Bibemi, Tcholliré, and Bantadjé. For Pinna et al. (1994) and Embui et al. (2013), these mineralizations are mainly located in fractured zones and are believed to have originated from batholithic granite formations. The gold concentrations can reach up to 1.12 g/t or even 2.79 g/t (Bouyo et al., 2015). However, mineral exploration processes are still ongoing within the study area.

3. Data and Methods

3.1. Data

Two ASTER images of L1T type were downloaded from the website https://earthexplorer.usgs.gov, covering the entire study area, and acquired on November 26 2006, corresponding to the beginning of the dry season with a complete absence of clouds. The L1T-type images have undergone correction for geometric effects through georeferencing to the UTM (Universal Transverse Mercator) WGS 84 coordinate system, as well as radiometric effects (Iwasaki & Tonooka, 2005). The ASTER Images consist of 14 spectral bands grouped into three domains: VNIR (Visible Near-Infrared), SWIR (Shortwave Infrared), and TIR (Thermal Infrared). In this study, we use ASTER satellite imagery to detect and identify hydrothermal alterations and map lineaments in the Poli area.

3.2. Methods

3.2.1. Preprocessing of ASTER Images

The two ASTER scenes were mosaicked, and subsequently, the study area was extracted. Although the image was downloaded during the dry season, it still shows some anomalies. The effects of clouds and aerosols have been eliminated through atmospheric correction carried out using the FLAASH module in ENVI. Furthermore, the vegetation effect has also been removed from the image.

3.2.2. Processing of ASTER Images

1) Lineaments mapping by DWT

The DWT represents an advancement in signal processing compared to the Fourier transformation. This method relies on small waves called wavelets, which can have varying frequencies and exhibit higher sensitivity to local variations (Gonzalez et al., 2007; Mallat, 1989). It has demonstrated significantly better re-

sults for mapping structures on satellite images (Bachofer et al., 2016). In this study, the PCA1 band, containing all the information from the ASTER image, is utilized for structure mapping. Once applied to the image, three component images are obtained: HC (Horizontal Component), VC (Vertical Component), and DC (Diagonal Component). Each of these images enhances structures along the N-S, E-W, and NE-SW directions, respectively. The lineaments are manually extracted from each image using the QGIS 3.28 software.

2) Image processing methods

a) Principal Component Analysis (PCA)

Multi-spectral data from different channels often contain similar information, and PCA transformations are used to reduce this data redundancy. The resulting "new" bands are referred to as components, allowing the reduction of the information contained in 5 or 6 channels to just three components while retaining over 90% of the original information. This is an effective technique for enhancing a multi-spectral image for geological and structural interpretation (Pour & Hashim, 2015). In this study, the PCA image obtained by combining SWIR and VNIR bands was used as a basis for identifying lineaments through DWT.

b) Band Ratio (BR) technique

The BR technique is based on mathematical operations that generate new images from selected bands. Its purpose is to mitigate the effects of topography and enhance contrast between mineral surfaces (Di Tommaso & Rubinstein, 2007). This operation allows the combination of information from multiple bands into a single band. Various permutations of VNIR, SWIR, and TIR bands have been employed to create band ratios. The band ratios (B5/B3 + B1/B2), (B4 + B6/B7)/(B8 + B9/B5), and (B14)/(B12) allow us to highlight iron oxides/hydroxides, hydroxyl-bearing minerals, and quartz index, respectively.

3.3. Methodology Workflow

In general, downloaded images undergo preprocessing for atmospheric corrections. Subsequently, step-by-step processing methods are applied to the image to extract structural information and hydrothermal alteration features. Structural mapping is performed using the wavelet transform algorithm programmed in Matlab, while hydrothermal alteration mapping is carried out using the band ratio method. The validation of the obtained results is conducted through two approaches. Firstly, by comparing the spectral signatures of alterations with those in the USGS (United States Geological Survey) database. Secondly, a field verification is conducted to identify and confirm the areas of alteration. The overall methodology approach for this work is illustrated in **Figure 2**.

4. Results

4.1. Lineament Mapping Using DWT

The ACP 1 image, containing the majority of information from the other bands, is used for lineament detection. Firstly, it is subjected to the DWT algorithm, which produces three main exploitable images as results.

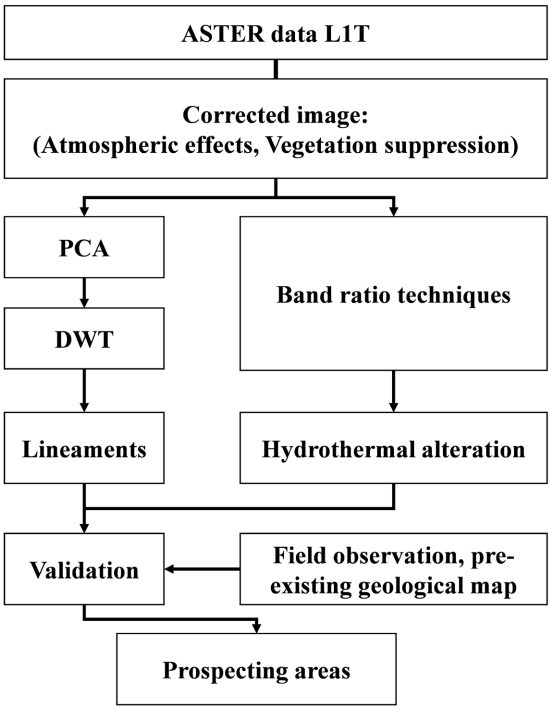

Figure 2. Flowchart showing the main steps of the methodology approach.

The Vertical Component (VC) (**Figure 3(a)**) highlights the N-S direction lineaments, the Horizontal Component (HC) (**Figure 3(b)**) emphasizes the E-W direction lineaments, the Diagonal Component (DC) (**Figure 3(c)**) highlights the NE-SW direction lineaments, and finally, the Approximation Component is similar to the input image. The lineaments are manually extracted from these images using the QGIS 3.28 software. After combining the lineaments extracted from the Vertical Component (VC), Horizontal Component (HC), and Diagonal Component (DC) components, a correction was applied by a true-color RGB (432) image with the aim of removing lineaments associated with roads and prevalent plantation alignments in the study area.

Figure 4(a) displays the distribution of lineaments in the study area. The obtained lineaments vary in size, ranging from 0.9 km to 5 km. The directional rose plot in **Figure 4(a)** shows three main directions: NE-SW, ENE-WSE, and E-W, with the NE-SW direction being predominant in the area. **Figure 4(b)** illustrates the density distribution of the lineaments. It can be observed that highly dense areas are mainly located at the center of the study area, including the Salaki, Poli, and Hoy regions, which exhibit a high density of lineaments. Additionally, a small region in the extreme Southwest of the Bantadjé area shows a high density of lineaments.

4.2. Hydrothermal Mapping

4.2.1. Oxides/Hydroxides

The detection of oxides and hydroxides was performed using the SWIR and VNIR bands of the ASTER image. According to Hung et al. (2005), these minerals

exhibit high reflectance in the visible domain between 0.78 µm and 0.86 µm and low reflectance between 0.4 µm and 0.9 µm. Oxides and hydroxides are typically identifiable in the field due to their reddish coloration resulting from rock alteration. This coloration is attributed to the presence of ferric and ferrous ions in the rocks. The band ratio (B5/B3 + B1/B2), as described by Ouhoussa et al. (2023), was also applied in our case to highlight oxide and hydroxide minerals in the study area. Spectral analysis of the identified zones revealed high reflectance values for wavelengths ranging from 0.1 to 1.0 µm (**Figure 5(b)**, Zone 1) and 0.5 to 1.1 µm (**Figure 5(b)**, Zone 2). By comparing these values with the spectral library of USGS, it was found that these zones likely correspond to hematite and limonite, respectively.

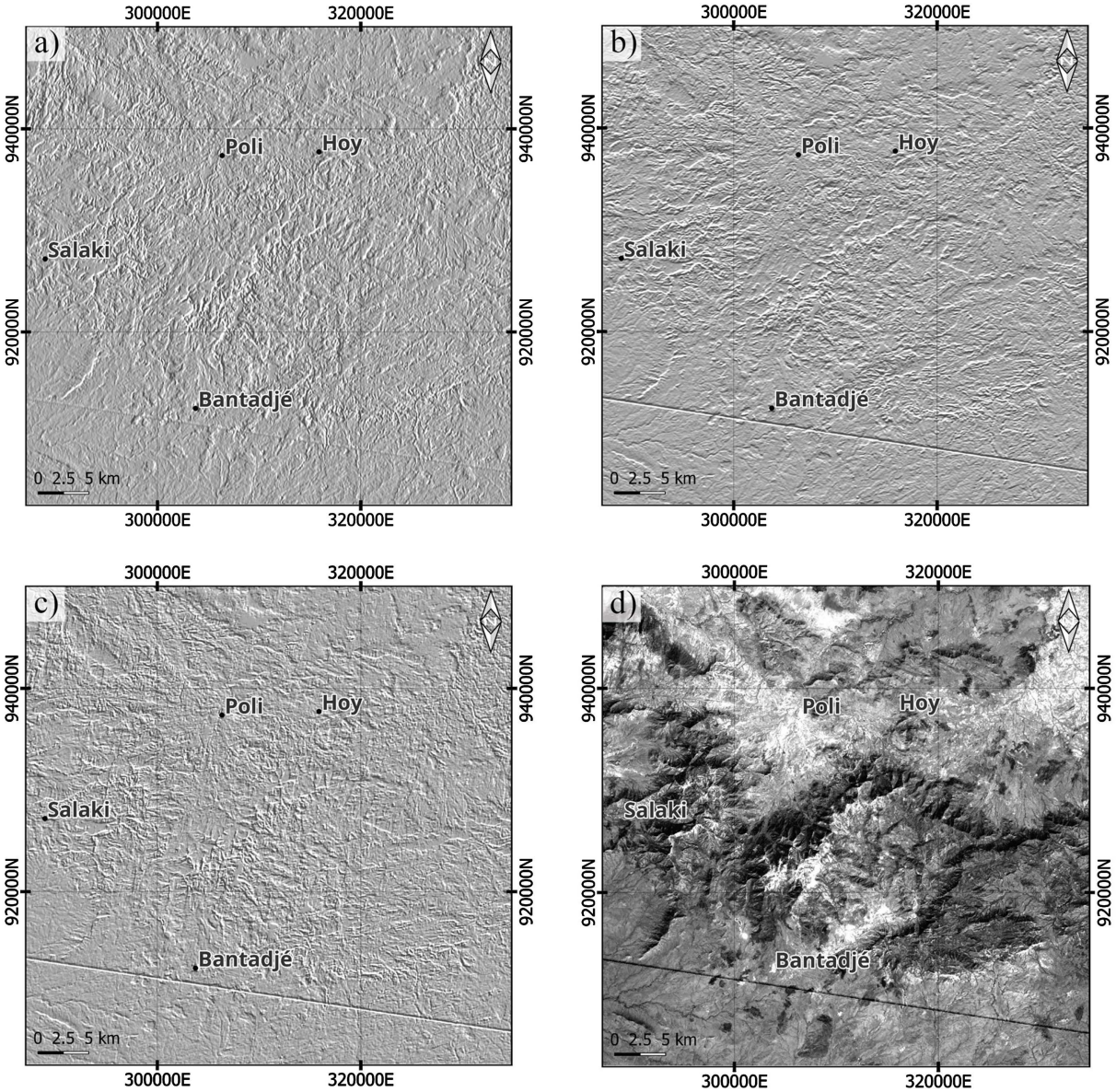

Figure 3. The DWT decomposition of PCA1 image: (a) Vertical details, (b) Horizontal details, (c) Diagonal details and (d) Approximation details at Level 1, respectively.

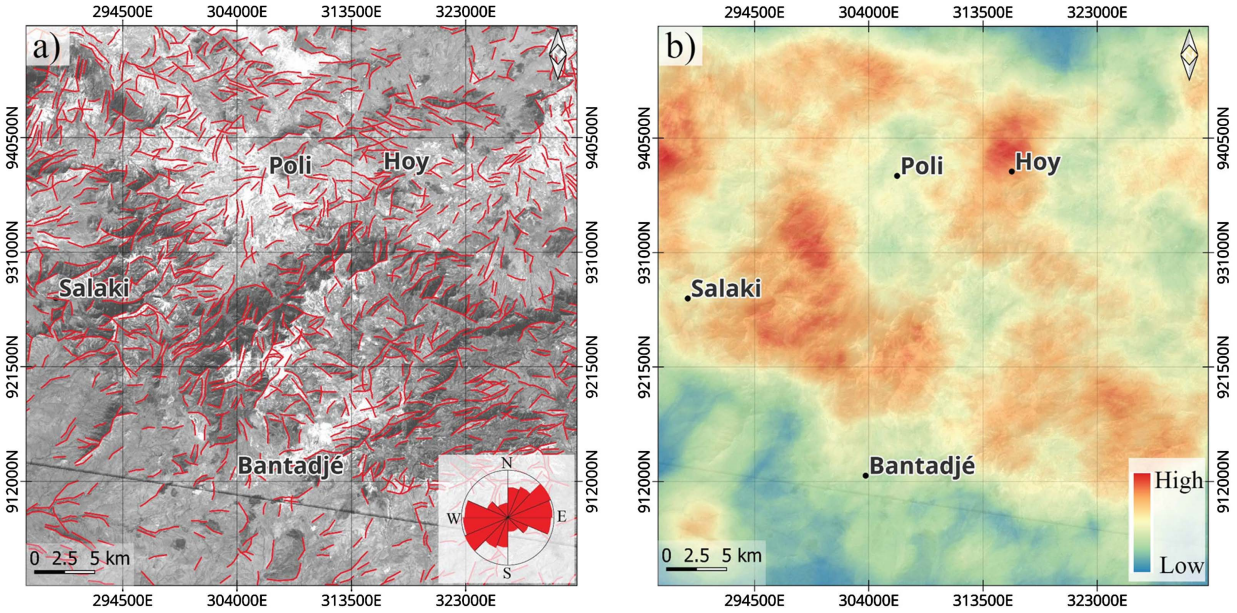

Figure 4. (a) Lineaments obtain from DWT, the associated rose diagram shows the direction of lineaments; (b) Density map of lineaments.

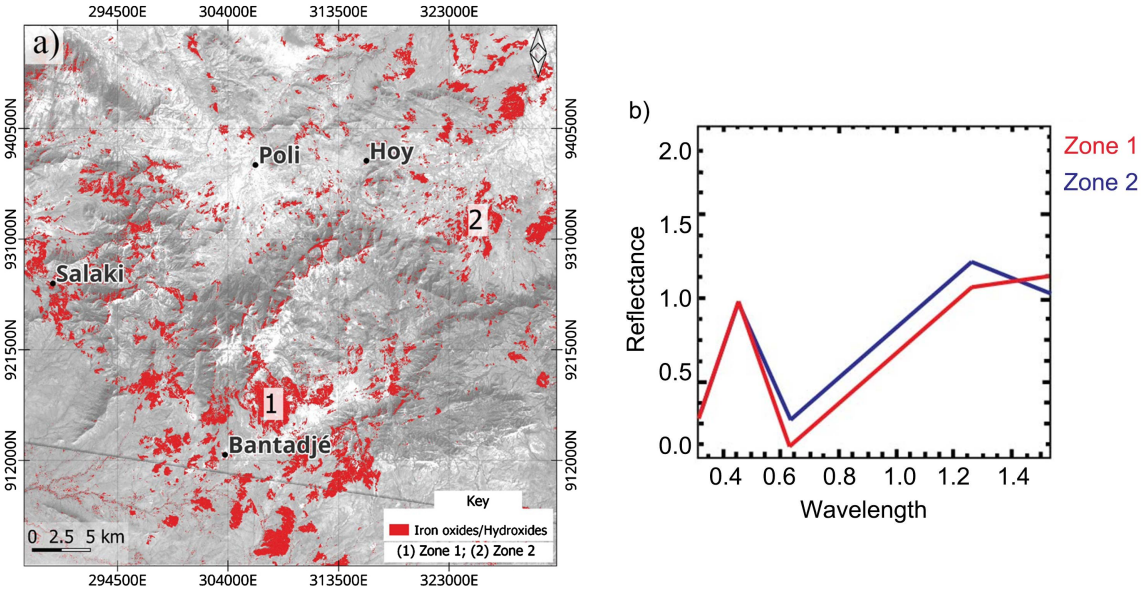

Figure 5. (a) Surfaces of iron oxides/hydroxides detected during the processing of the ASTER images; (b) Spectral signatures of a few pixels belonging to areas rich in iron oxides and hydroxides.

The map in Figure 5(a) displays the distribution of these minerals in red color, showing a concentration of these minerals at the center of the study area, mainly on the slopes of the hills. These areas are identifiable on the field by their distinct red coloration, as seen from a distance (Figure 6). Based on the geological map and field observations, we can infer that these indicators are predominantly associated with the formations of schists and gneisses in the study area. Their origins are likely linked to the alteration of primary minerals such as magnetite and pyrite.

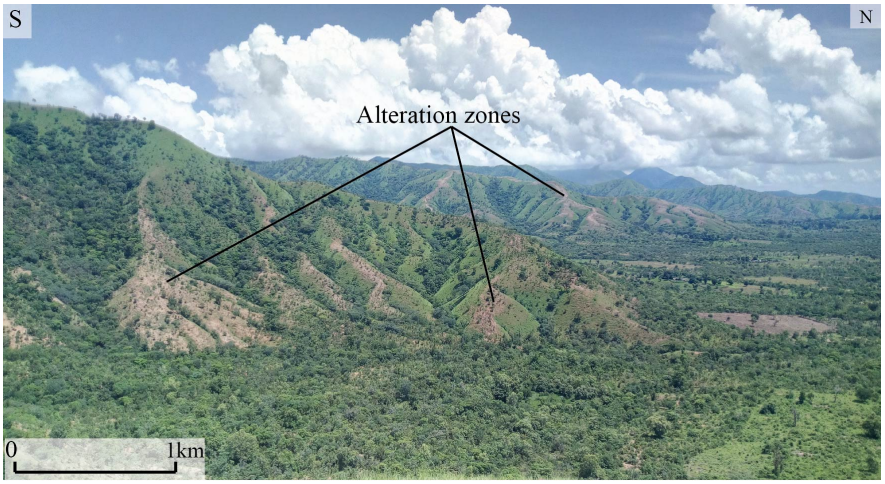

Figure 6. Areas of alteration on the hillsides.

4.2.2. Hydroxyl Bearing-Minerals

The alteration of hydroxyl-bearing minerals mainly consists of clays, micas, and talc carbonates. The detection of these minerals is primarily done using the SWIR bands. Hydroxyl-bearing minerals exhibit significant reflectance in the wavelengths 1.5 - 1.6 μm and 2.1 - 2.3 μm (Sultan et al., 1987; Eldosouky et al., 2017; Mars & Rowan, 2006; Amer et al., 2010). The band ratio (B4 + B6/B7)/(B8 + B9/B5) (Ouhoussa et al., 2023) has yielded excellent results and enabled the identification of clay-rich alteration zones. Spectral analysis of the identified zones reveals three areas with different reflectance values. The first zone exhibits high reflectance between wavelengths 2.0 μm and 2.2 μm (**Figure 7(b)**, Zone 1), while the second zone shows increased reflectance between 1.5 μm and 2 μm (**Figure 7(b)**, Zone 2). After comparison with the USGS Library, it is apparent that these zones correspond to the response of chlorites and muscovites, respectively. The third zone (**Figure 7(b)**, Zone 3) displays low reflectance between wavelengths 2.2 μm and 2.5 μm, which would be indicative of epidote according to the USGS Library. Based on the geological map and field observations, these pixels are found to coincide with clay-rich areas, mainly in the valleys (**Figure 7(d)**), outcrops of muscovite-rich schists (**Figure 7(c)**), and sometimes heavily altered granitic mountainous regions.

4.2.3. Quartz Index

Rock formations rich in quartz elements exhibit a high absorption of SiO_2 in the TIR (Thermal Infrared) domain (Di Tommaso & Rubinstein, 2007; Safari et al., 2017). Therefore, the TIR bands have been employed to identify areas with quartz indices. The normalized formula (B14)/(B12) from Rowan and Mars (2003) was used to determine the quartz-rich zones. Spectral analysis of two areas revealed a very strong reflectance between wavelengths of 9 μm to 11 μm (**Figure 8(b)**).

The observation of the map in the figure shows an abundance of quartz indices in the study area. The quartz indices are more densely concentrated in the

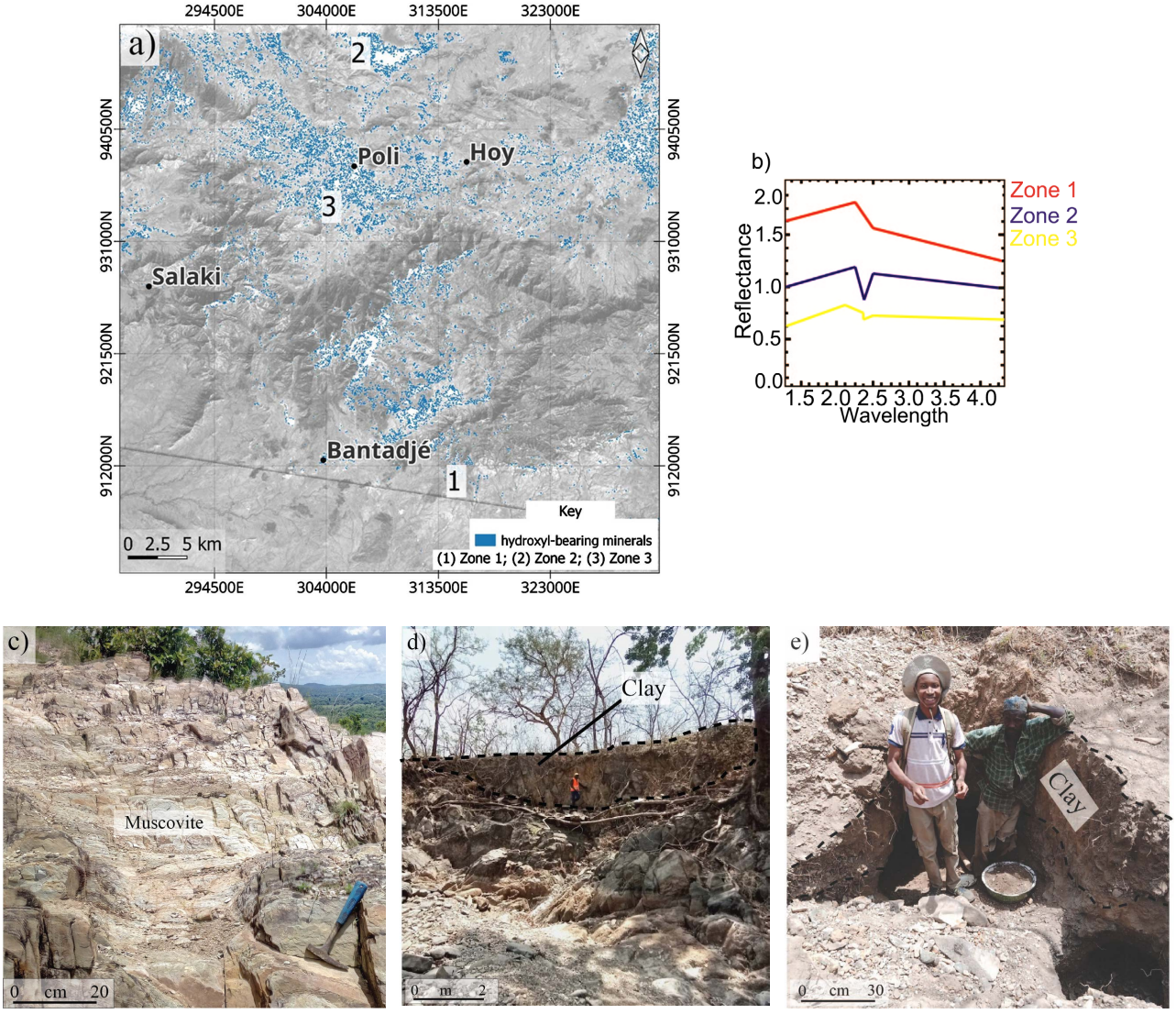

Figure 7. (a) Surfaces of iron hydroxyl-bearing minerals detected during the processing of the ASTER image; (b) Spectral signatures of a few pixels belonging to areas rich in hydroxyl-bearing minerals; (c) Muscovite on a schist; (d) Clay bed in the lowlands; (e) Clay layer in an artisanal gold mining site.

central area between Bantadjé village and the city of Poli, which corresponds to the response of granite mountainous formations covering this area (**Figure 9(c)**). The concentration in the extreme northwest of the study area corresponds to the response of the mountainous massif of Mount Gode. The areas with low concentrations would correspond to the response of quartzites, quartz veins in gneissic and schist rocks (**Figure 9(d)**), and quartz pebbles present in the watercourses (**Figure 9(e)**).

5. Discussion

Hydrothermal fluids are primarily transported through geological structures such as linear features (faults, fractures) (Koike et al., 1998). Additionally, the contact zones between multiple linear features can be considered as fractures

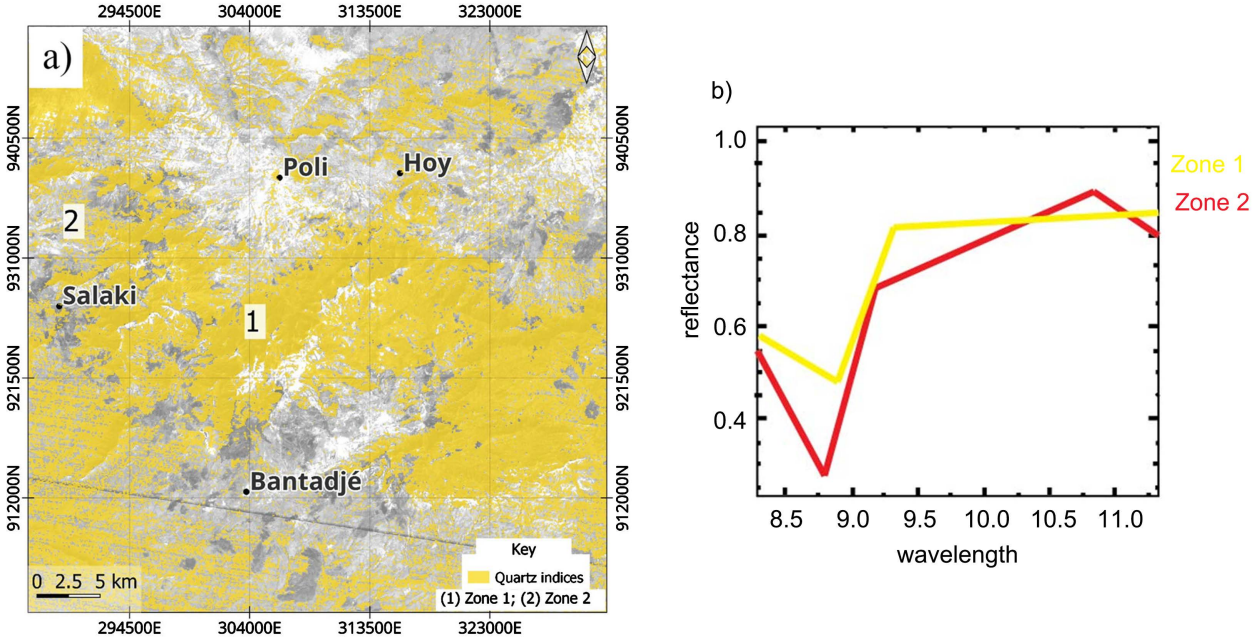

Figure 8. Surfaces of quartz index detected during the processing of the ASTER image: (a) Superimposition of the surfaces detected with PC1; (b) Spectral signatures of a few pixels belonging to areas rich in quartz (SiO_2).

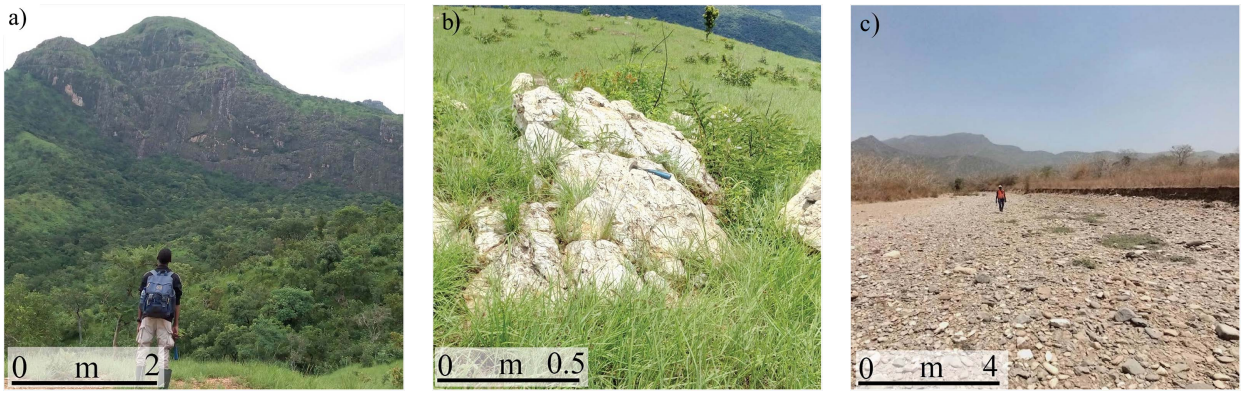

Figure 9. (a) Granite outcrop on Mont Kitongo; (b) Quartzite outcrop; (c) Quartz pebbles in a tributary of the Bantadjé mayo.

(Koike et al., 1998). In the context of this study, the linear features obtained through ASTER data processing using DWT indicate a prevailing NE-SW direction, which corresponds to the main structural trend in the Poli area (Dumont et al., 1985; Njel, 1986; Nomo et al., 2017). This direction is followed by E-W and ENE-WSE orientations, as shown in the directional rose diagram in **Figure 4(a)**. The significant presence of fractures suggests good permeability for the circulation of hydrothermal fluids and groundwater. Moreover, these linear features serve as indicators that could be followed in gold exploration, as the formation of secondary minerals (such as quartz, chlorite, and epidote) is closely linked to their presence and influence. The density map of linear features (**Figure 10(a)**) has been divided into areas of high and low linear feature density. Overlaying this map with known mining indices and those observed in the field (**Figure 10(a)**) reveals a strong correlation between areas of high density and mineralization

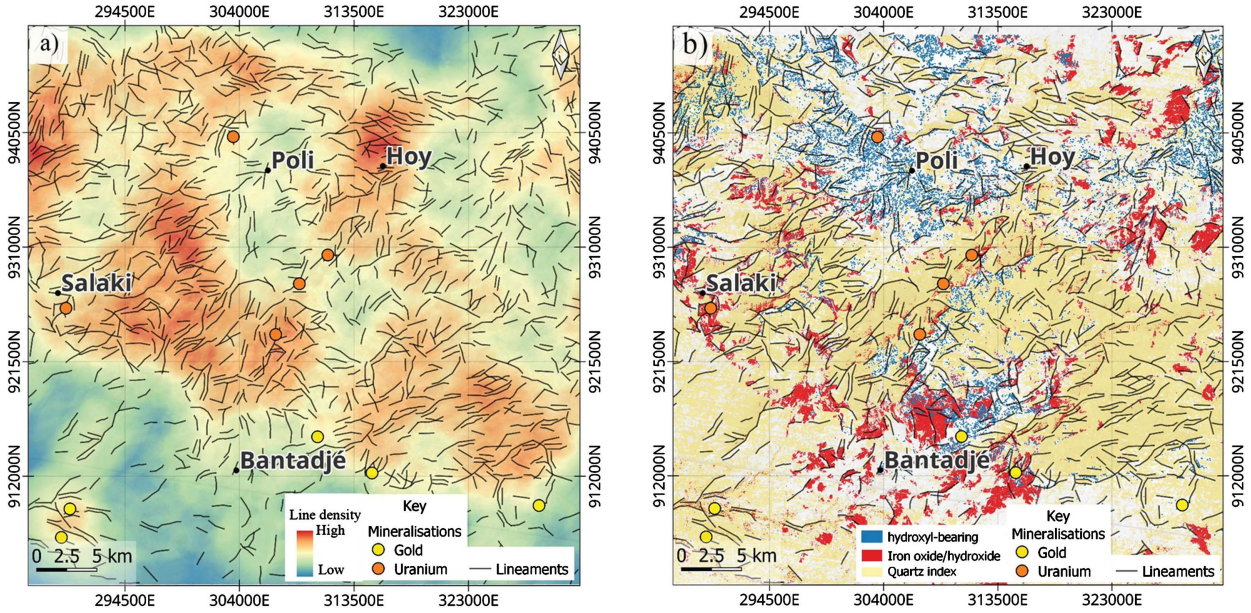

Figure 10. (a) Density map of lineaments coupled with mining indices in the study area; (b) Map showing the coupling of hydrothermal alteration and mining indices.

indices. High-density zones can be considered to have a high probability of mineralization, while low-density areas may have a low probability, and moderate probabilities are associated with the intermediate zones. Hydrothermal alteration mapping has enabled the identification of zones rich in oxides/hydroxides (hematite, limonite), hydroxide-bearing minerals (epidote, chlorite, and muscovite), and quartz indicators. Overall, these findings highlight the potential of linear features as important pathways for hydrothermal fluids and groundwater, and their correlation with mineralization indices provides valuable insights for gold exploration. The mapping of hydrothermal alteration zones offers further indications of potential mineral-rich areas in the study region.

A strong correlation has been observed between the obtained indices and the lithological formations of the study area. According to Nomo et al. (2017), Toteu et al. (2001), Kouske et al. (2012) and Tchameni et al. (2013), the Poli zone is associated with two stages of granitic intrusions that have led to the enrichment of the area in uranium and gold. Additionally, the works of Anaba Fotze et al. (2019), and Ketchaya et al. (2021) have demonstrated a strong relationship between mineralization and hydrothermal alteration in the North Cameroon. In the context of this study, the superposition of hydrothermal alteration zones with known mineralization indices shows a significant correlation (**Figure 10(b)**). The combination of obtained lineament densities, different oxide/hydroxide alteration indices, and hydroxyl-bearing minerals can serve as a guide for enhancing mining exploration in the study area. Zones, where high lineament densities coincide with the presence of alteration indices, are considered most favorable. Thus, areas around the Salaki village, north of the Bantadjé village, and near the Hoy and Poli villages hold the most promise for future exploration efforts.

6. Conclusion

The aim of this study was to perform structural and hydrothermal alteration mapping using ASTER images of the Poli region and its surroundings. To achieve this objective, a specific methodology was followed. Firstly, the two ASTER images were mosaicked, and the area was delimited and extracted. Next, the obtained scene was corrected for atmospheric effects, and vegetation influence was removed. Subsequently, these images were subjected to discrete wavelet transformation algorithms, which highlighted the main lineaments present in the study area. Thirdly, band ratio methods were applied to the VNIR, SWIR, and TIR bands of the images to determine iron oxide indices. Among these indices, hematite and limonite were identified through spectral analysis. Additionally, indices of hydroxyl-bearing minerals such as epidotes, chlorites, and muscovites, as well as quartz index, were identified. The analysis of the obtained lineaments allowed for the identification of three main directions: NE-SW, ENE-WSW, and E-W, with a predominance of the NE-SW direction. Regarding hydrothermal alteration, the identified indices covered almost the entire study area and showed a good correlation with lithological data. The intersection of the obtained lineaments with hydrothermal alteration indices revealed a strong correlation between existing mining indices and those observed in the field. Mineralization zones generally coincided with areas of high lineament density exhibiting significant hydrothermal alteration. These findings suggest that the obtained results can serve as a guide for the exploration of gold and uranium mineralizations in the Poli area. We also suggest additional fieldwork and ground geophysics (resistivity and induced polarization) in areas identified as being of interest. This additional work will increase the knowledge of the depths of mineralized gravels in gold-bearing zones and will help to detect structures (veins) carrying uranium mineralization.

Acknowledgements

The authors are grateful to Professor ABDOUL WAHABOU, Director of the School of Geology and Mining Engineering, University of Ngaoundéré, for providing the infrastructural facilities. We are also thankful to those people who helped in different stages of this work.

Funding

This research did not receive any specific grant from funding agencies in the public, commercial, or not-for-profit sectors.

Data Availability

The data sets used and/or analyzed during the current study are available from the corresponding author upon reasonable request.

Conflicts of Interest

The authors declare no competing interests.

References

Abdelsalam, M. G., Gao, S. S., & Liégeois, J. (2011). Upper Mantle Structure of the Saharan Metacraton. *Journal of African Earth Sciences, 60,* 328-336. https://doi.org/10.1016/j.jafrearsci.2011.03.009

Abdelsalam, M. G., Liégeois, J. P., & Stern, R. J. (2002). The Saharan Metacraton. *Journal of African Earth Sciences, 34,* 119-136. https://doi.org/10.1016/S0899-5362(02)00013-1

Affaton, P., Rahaman, M. A., Trompette, R., & Sougy, J. (1991). The Dahomeyide Orogen: Tectonothermal Evolution and Relationships with the Volta Basin. In R. D. Dallmeyer, & J. P. Lécorché (Eds.), *The West African Orogens and Circum-Atlantic Correlatives* (pp. 107-122). Springer. https://doi.org/10.1007/978-3-642-84153-8_6

Amer, R., Kusky, T., & Ghulam, A. (2010). Lithological Mapping in the Central Eastern Desert of Egypt Using ASTER Data. *Journal of African Earth Sciences, 56,* 75-82. https://doi.org/10.1016/j.jafrearsci.2009.06.004

Anaba Fotze, Q. M., Lordon, A. E. D., Penaye, J., Sep, J. P., & Fru, M. I. N. (2019). Mapping Hydrothermal Alteration Targets from Landsat 8 OLI/TIRS and Magnetic Data Using Digital Image Processing Techniques in Garoua, North Cameroon. *Journal of Geosciences and Geomatics, 7,* 28-41. https://doi.org/10.12691/jgg-7-1-4

Bachofer, F., Quénéhervé, G., Zwiener, T., Maerker, M., & Hochschild, V. (2016). Comparative Analysis of Edge Detection Techniques for SAR Images. *European Journal of Remote Sensing, 49,* 205-224. https://doi.org/10.5721/EuJRS20164912

Baid, S., Tabit, A., Algouti, A., Algouti, A., Nafouri, I., Souddi, S., Aboulfaraj, A., Ezzahzi, S., & Elghouat, A. (2023). Lithological Discrimination and Mineralogical Mapping Using Landsat-8 OLI and ASTER Remote Sensing Data: Igoudrane Region, Jbel Saghro, Anti Atlas, Morocco. *Heliyon, 9,* E17363. https://doi.org/10.1016/j.heliyon.2023.e17363

Bessoles, B., & Trompette, M. (1980). *Géologie de l'Afrique: La chaîne Panafricaine, "Zone mobile d'Afrique centrale (partie sud) et Zone mobile soudanaise"* (pp. 19-80). Mémoires du Bureau de Recherches Géologiques et Minières, No. 92, Editions B.R.G.M.

Bouyo, M. H., Penaye, J., Barbey, P., Toteu, S., & Wandji, P. (2013). Petrology of High-Pressure Granulite Facies Metapelites and Metabasites from Tcholliré and Banyo Regions: Geodynamic Implication for the Central African Fold Belt (CAFB) of North-Central Cameroon. *Precambrian Research, 224,* 412-433. https://doi.org/10.1016/j.precamres.2012.09.025

Bouyo, M. H., Zhao, Y., Penaye, J., Zhang, S., & Njel, U. O. (2015). Neoproterozoic Subduction-Related Metavolcanic and Metasedimentary Rocks from the Rey Bouba Greenstone Belt of North-Central Cameroon in the Central African Fold Belt: New Insights into a Continental Arc Geodynamic Setting. *Precambrian Research, 261,* 40-53. https://doi.org/10.1016/j.precamres.2015.01.012

Deroin, J. P. (2019). An Overview on 40 Years of Remote Sensing Geology Based on Arab Examples. In A. Bendaoud, Z. Hamimi, M. Hamoudi, S. Djemai, & B. Zoheir (Eds.), *The Geology of the Arab World—An Overview* (pp. 427-453). Springer International Publishing. https://doi.org/10.1007/978-3-319-96794-3_12

Di Tommaso, I., & Rubinstein, N. A. (2007). Hydrothermal Alteration Mapping Using ASTER Data in the Infiernillo Porphyry Deposit, Argentina. *Ore Geology Reviews, 32,* 275-290. https://doi.org/10.1016/j.oregeorev.2006.05.004

Dumont, J. F., Toteu, S. F., & Penaye, J. (1985). Ensembles structuraux et principales phases de déformations panafricaines dans la zone mobile du Nord Cameroun, région de Poli. *Revue des Sciences et Techniques, Série Sciences de la Terre, 1,* 9-23.

Eldosouky, A. M., Abdelkareem, M., & Elkhateeb, S. O. (2017). Integration of Remote

Sensing and Aeromagnetic Data for Mapping Structural Features and Hydrothermal Alteration Zones in Wadi Allaqi Area, South Eastern Desert of Egypt. *Journal of African Earth Sciences, 130,* 28-37. https://doi.org/10.1016/j.jafrearsci.2017.03.006

Embui, V. F., Omang, B. O., Che, V. B., Nforba, M. T., & Suh, C. E. (2013). Gold Grade Variation and Stream Sediment Geochemistry of the Vaimba-Lidi Drainage System Northern Cameroon. *Journal of Natural Science, 5,* 282-290. https://doi.org/10.4236/ns.2013.52A040

Gonzalez, R. C., Woods, R. E., & Eddins, S. (2007). *Digital Image Processing Using MATLAB* (3rd ed.). Prentice Hall Press. https://www.mathworks.com/academia/books/digital-image-processing-using-matlab-gonzalez.html

Hung, L. Q., Batelaan, O., & De Smedt, F. (2005). Lineament Extraction and Analysis, Comparison of LANDSAT ETM and ASTER Imagery. Case Study: Suoimuoi Tropical Karst Catchment, Vietnam. In M. Ehlers, & U. Michel (Eds.), *Proceedings Remote Sensing for Environmental Monitoring, GIS Applications, and Geology V* (Vol. 5983, 59830T). International Society for Optics and Photonics (SPIE). https://doi.org/10.1117/12.627699

Iwasaki, A., & Tonooka, H. (2005). Validation of a Crosstalk Correction Algorithm for ASTER/SWIR. *IEEE Transactions on Geoscience and Remote Sensing, 43,* 2747-2751. https://doi.org/10.1109/TGRS.2005.855066

Ketchaya, Y. B., Dong, G., Fotze, Q. M. A., Carrino, T. A., Mandeng, E. P. B., Lemdjou, Y. B., Assie, K. R., Yannah, M., & Wadjou, J. W. (2021). Integration of Landsat 8, Gravity, and Field Data for Exploration of Gold Mineralization in Gamba District, Northern Cameroon. *Geological Journal, 56,* 4788-4808. https://doi.org/10.1002/gj.4197

Koike, K., Nagano, S., & Kawaba, K. (1998). Construction and Analysis of Interpreted Fracture Planes through Combination of Satellite-Image Derived Lineaments and Digital Elevation Model Data. *Computers and Geosciences, 24,* 573-583. https://doi.org/10.1016/S0098-3004(98)00021-1

Kouske, A. P., Suh, C. E., Ghogomu, R. T., & Ngako, V. (2012). Na-Metasomatism and Uranium Mineralization during a Two-Stage Albitization at Kitongo, Northern Cameroon: Structural and Geochemical Evidence. *International Journal of Geosciences, 3,* 258-279. https://doi.org/10.4236/ijg.2012.31028

Lasserre, M., & Soba, D. (1979). Migmatisation d'age panafricain au sein des formations camerounaises appartenant à la zone mobile d'Afrique centrale. *Comptes Rendus Sommaires Societe Geologique de France, 2,* 64-68.

Mallat, S. (1989). A Theory for Multiresolution Signal Decomposition: The Wavelet Representation. *IEEE Transactions on Pattern Analysis and Machine Intelligence, 11,* 674-693. https://doi.org/10.1109/34.192463

Mars, J., & Rowan, L. C. (2006). Regional Mapping of Phyllic- and Argillic-Altered Rocks in the Zagros Magmatic Arc, Iran, Using Advanced Spaceborne Thermal Emission and Reflection Radiometer (ASTER) Data and Logical Operator Algorithms. *Geosphere, 2,* 161-186. https://doi.org/10.1130/GES00044.1

Negue, E. N., Tchameni, R., Vanderhaeghe, O., Sun, F., Barbey, P., Tekoum, L., Tchunte, P. M. F., Eglinger, A., & Fouotsa, N. A. S. (2017). Structure and LA-ICP-MS Zircon U-Pb Dating of Syntectonic Plutons Emplaced in the Pan-African Banyo-Tcholliré Shear Zone (Central North Cameroon). *Journal of African Earth Sciences, 131,* 251-271. https://doi.org/10.1016/j.jafrearsci.2017.04.002

Ngnotué, T., Nzenti, J. P., Barbey, P., & Tchoua, F. M. (2000). The Ntui-Betamba High-Grade Gneisses: A Northward Extension of the Pan-African Yaoundé Gneisses in Ca-

meroon. *Journal of African Earth Sciences, 31,* 369-381. https://doi.org/10.1016/S0899-5362(00)00094-4

Njanko, T., Nédélec, A., Maurice, K., Siqueira, R., & Esteban, L. (2010). Emplacement and Deformation of the Fomopéa Pluton: Implication for the Pan-African History of Western Cameroon. *Journal of Structural Geology, 32,* 306-320. https://doi.org/10.1016/j.jsg.2009.12.007

Njel, U. O. (1986). Paléogéographie d'un segment de l'orogenèse panafricaine: La ceinture volcano-sédimentaire de Poli (Nord Cameroun). *Comptes Rendus de l'Académie des Sciences, Paris, 303,* 1737-1742.

Nomo, E. N., Tchameni, R., Vanderhaeghe, O., Sun, F., Barbey, P., Tekoum, L., Tchunte, P. M. F., Eglinger, A., & Fouotsa, N. A. S. (2017). Structure and LA-ICP-MS Zircon U-Pb Dating of Syntectonic Plutons Emplaced in the Pan-African Banyo-Tcholliré Shear Zone (Central North Cameroon). *Journal of African Earth Sciences, 131,* 251-271. https://doi.org/10.1016/j.jafrearsci.2017.04.002

Nzenti, J. P., Kapajika, B., Warner, G., & Lubala, T. R. (2006). Synkinematic Emplacement of Granitoids in a Pan-African Shear Zone in Central Cameroon. *Journal of African Earth Sciences, 45,* 74-86. https://doi.org/10.1016/j.jafrearsci.2006.01.005

Ouhoussa, L., Ghafiri, A., Aissi, L. B., & Es-sabbar, B. (2023). Integrating Aster Images Processing and Fieldwork for Identification of Hydrothermal Alteration Zones at the Oumjrane-Boukerzia District, Moroccan Anti-Atlas. *Open Journal of Geology, 13,* 171-188. https://doi.org/10.4236/ojg.2023.132008

Ouhoussa, L., Ghafiri, A., Benaissi, L., Es-sabbar, B., & Si Mhamdi, H. (2022). Litho-structural Mapping Using Landsat OLI Images and Field Investigations in the Oumjrane-Boukerzia Mining District, Eastern Anti-Atlas, Morocco. *Iraqi Geological Journal, 55,* 14-33. https://doi.org/10.46717/igj.55.2C.2ms-2022-08-15

Penaye, J., Kröner, A., Toteu, S., Van Schmus, W. R., & Doumnang, J. (2006). Evolution of the Mayo Kebbi Region as Revealed by Zircon Dating: An Early (ca. 740Ma) Pan-African Magmatic Arc in Southwestern Chad. *Journal of African Earth Sciences, 44,* 530-542. https://doi.org/10.1016/j.jafrearsci.2005.11.018

Penaye, J., Toteu, S. F., Van Schmus, W. R., & Nzenti, J. P. (1993). U-Pb and Sm-Nd Preliminary Geochronology Data on the Yaoundé Series, Cameroon: Re-Interpretation of the Granulitic Rocks as the Suture of Collision in the "Centrafrican" Belt. *Comptes Rendus de l'Académie des Sciences de Paris, 317,* 789-794.

Pinna, P., Calvez, J. Y., Abessolo, A., Angel, J. M., Mekoulou, T., Mananga, G., & Vernhet, Y. (1994). Neoproterozoic Events in the Tcholliré Area: Pan-African Crustal Growth and Geodynamics in Central-Northern Cameroon (Adamawa and North Provinces). *Journal of African Earth Sciences, 18,* 347-353. https://doi.org/10.1016/0899-5362(94)90074-4

Pour, A. B., & Hashim, M. (2015). Hydrothermal Alteration Mapping from Landsat-8 Data, Sar Cheshmeh Copper Mining District, South-Eastern Islamic Republic of Iran. *Journal of Taibah University for Science, 9,* 155-166. https://doi.org/10.1016/j.jtusci.2014.11.008

Rowan, L. C., & Mars, J. (2003). Lithologic Mapping in the Mountain Pass, California Area Using Advanced Spaceborne Thermal Emission and Reflection Radiometer (ASTER) Data. *Remote Sensing of Environment, 84,* 350-366. https://doi.org/10.1016/S0034-4257(02)00127-X

Safari, M., Maghsoudi, A., & Pour, A. B. (2017). Application of Landsat-8 and ASTER Satellite Remote Sensing Data for Porphyry Copper Exploration: A Case Study from Shahr-e-Babak, Kerman, South of Iran. *Geocarto International, 33,* 1186-1201.

https://doi.org/10.1080/10106049.2017.1334834

Sultan, M. (1987). Lithologic Mapping in Arid Regions with Landsat Thematic Mapper Data: Meatiq Dome, Egypt. *GSA Bulletin, 99,* 748-762. https://doi.org/10.1130/0016-7606(1987)99<748:LMIARW>2.0.CO;2

Tchameni, R., Doumnang, J., Deudibaye, M., & Branquet, Y. (2013). On the Occurrence of Gold Mineralization in the Pala Neoproterozoic Formations, South-Western Chad. *Journal of African Earth Sciences, 84,* 36-46. https://doi.org/10.1016/j.jafrearsci.2013.03.002

Toteu, S. F., Penaye, J., & Poudjom, D. Y. (2004). Geodynamic Evolution of the Pan-African Belt in Central Africa with Special Reference to Cameroon. *Canadian Journal of Earth Sciences, 41,* 73-85. https://doi.org/10.1139/e03-079

Toteu, S. F., Penaye, J., Deloule, E., Van Schmus, W. R., & Tchameni, R. (2006). Diachronous Evolution of Volcano-Sedimentary Basins North of the Congo Craton: Insights from U-Pb Ion Microprobe Dating of Zircons from the Poli, Lom and Yaoundé Groups (Cameroon). *Journal of African Earth Sciences, 44,* 428-442. https://doi.org/10.1016/j.jafrearsci.2005.11.011

Toteu, S. F., Van Schmus, W. R., Penaye, J., & Michard, A. (2001). New U-Pb and Sm-Nd Data from North-Central Cameroon and Its Bearing on the Pre-Pan African History of Central Africa. *Precambrian Research, 108,* 45-73. https://doi.org/10.1016/S0301-9268(00)00149-2